European Radiology (2019) 29:6762–6771
https://doi.org/10.1007/s00330-019-06322-5

EMERGENCY RADIOLOGY

Virtual versus true non-contrast dual-energy CT imaging for the diagnosis of aortic intramural hematoma

Salim Si-Mohamed[1,2] · Nicolas Dupuis[1,2,3] · Valérie Tatard-Leitman[1] · David Rotzinger[4] · Sara Boccalini[2] · Matthias Dion[1,2,3] · Alain Vlassenbroek[5] · Philippe Coulon[6] · Yoad Yagil[7] · Nadav Shapira[7] · Philippe Douek[1,2] · Loic Boussel[1,2]

Received: 11 February 2019 / Revised: 24 May 2019 / Accepted: 11 June 2019 / Published online: 1 July 2019

Abstract

Purpose To assess whether virtual non-contrast (VNC) images derived from contrast dual-layer dual-energy computed tomography (DL-DECT) images could replace true non-contrast (TNC) images for aortic intramural hematoma (IMH) diagnosis in acute aortic syndrome (AAS) imaging protocols by performing quantitative as well as qualitative phantom and clinical studies.

Materials and methods Patients with confirmed IMH were included retrospectively in two centers. For in vitro imaging, a custom-made phantom of IMH was placed in a semi-anthropomorphic thorax phantom (QRM GmbH) and imaged on a DL-DECT at 120 kVp under various conditions of patient size, radiation exposure, and reconstruction modes. For in vivo imaging, 21 patients (70 ± 13 years) who underwent AAS imaging protocols at 120 kVp were included. In both studies, contrast-to-noise ratio (CNR) between hematoma and lumen was compared using a paired *t* test. Diagnostic confidence (1 = non-diagnostic, 4 = exemplary) for VNC and TNC images was rated by two radiologists and compared. Effective radiation doses for each acquisition were calculated.

Results In both the phantom and clinical studies, we observed that the CNRs were similar between the VNC and TNC images. Moreover, both methods allowed differentiating the hyper-attenuation within the hematoma from the blood. Finally, we obtained equivalent high diagnostic confidence with both VNC and TNC images (VNC = 3.2 ± 0.7, TNC = 3.1 ± 0.7; $p = 0.3$). Finally, by suppressing TNC acquisition and using VNC, the mean effective dose reduction would be 40%.

Conclusion DL-DECT offers similar performances with VNC and TNC images for IMH diagnosis without compromise in diagnostic image quality.

Key Points

- *Dual-layer dual-energy CT enables virtual non-contrast imaging from a contrast-enhanced acquisition.*
- *Virtual non-contrast imaging with dual-layer dual-energy CT reduces the number of acquisitions and radiation exposure in acute aortic syndrome imaging protocol.*
- *Dual-layer dual-energy CT has the potential to become a suitable imaging tool for acute aortic syndrome.*

Salim Si-Mohamed and Nicolas Dupuis contributed equally to this work.

Electronic supplementary material The online version of this article (https://doi.org/10.1007/s00330-019-06322-5) contains supplementary material, which is available to authorized users.

✉ Salim Si-Mohamed
salimaymeric@gmail.com; salim.si-mohamed@chu-lyon.fr

[1] Univ Lyon, INSA-Lyon, Université Claude Bernard Lyon 1, UJM-Saint Etienne, CNRS, Inserm, CREATIS UMR 5220, U1206, F-69621 Lyon, France

[2] Radiology Department, Hospices Civils de Lyon, CHU Louis Pradel, 59 Boulevard Pinel, 69500 Bron, France

[3] Anatomy Lab, Rockefeller Faculty, Lyon Est, Lyon, France

[4] Department of Diagnostic and Interventional Radiology, Lausanne University Hospital , Lausanne, Switzerland

[5] CT Clinical Science, Best, Netherlands

[6] CT Clinical Science, Philips, Suresnes, France

[7] Global Advanced Technologies, CT, Philips, Haifa, Israel

Keywords Tomography, x-ray computed · Humans · In vitro · Acute disease · Aorta

Abbreviations

AAS	Acute aortic syndrome
CNR	Contrast-to-noise ratio
CTA	CT angiography
CTDI*vol*	Volume CT dose index
DL-DECT	Dual-layer dual-energy computed tomography
DLP	Dose-length product
DS-DECT	Dual-source dual-energy computed tomography
IMH	Intramural hematoma
ROI	Regions of interest
SD	Standard deviations
TNC	True non-contrast
VNC	virtual non-contrast
WED	Water-equivalent diameter

Introduction

Aortic intramural hematoma (IMH) is a life-threatening condition that belongs to the spectrum of acute aortic syndrome (AAS). It is caused by micro-intimal tear or rupture of the vasa vasorum that creates a hemorrhage into the aortic media and thickens the aortic wall. Between 16% and 47% of IMH will progress to dissection often leading to patient's death [1]. Therefore, it is essential to promptly diagnose IMH in order to perform emergency surgery when necessary [2].

Today, dual-phase CT angiography (CTA) is considered the best tool available for IMH diagnosis [3, 4]. Indeed, while IMH appears as a circumference of hyperattenuation on non-contrast CT images, it is undetectable on contrast CT images due to the masking effect of iodine [1, 5–7]. Therefore, dual-phase CTA requires a non-contrast scan for the detection of aortic IMH and a contrast scan during the arterial phase for the detection of intimal tears, extension of an aortic disease, contrast leakage, and visceral ischemia [2, 4, 8, 9]. However, a disadvantage of dual-phase CTA is the higher radiation dose [10, 11]. To decrease the dose, Knollman et al have proposed to replace the non-contrast phase using a threshold to differentiate the IMH from the aortic lumen [12]. Unfortunately, this method highly depends on attenuation levels, which are affected by various factors such as tube voltage, patient size, or beam-hardening effects that make the diagnosis of thin IMH particularly difficult due to the high concentration of iodine within the blood pool [13].

Dual-energy CT (DECT), comparing two different energy levels, discriminates materials of different effective atomic numbers [14–18]. Post-processing can create virtual non-contrast images (VNC) that simulate true non-contrast images (TNC) by subtracting the attenuation due to iodine from the contrast-enhanced images [19, 20]. However, the comparability of VNC with TNC images depends on the accuracy of iodine quantification. For example, in the study of Hua et al [19], iodine accuracy is within 0.3 mg/mL (median) with a maximal deviation of 0.5 mg/mL. This translates into variation of up to 10–15 HU, in line with the results of previous studies [19, 21–26]. Therefore, since VNC is only an approximation of TNC, it is important to check the usefulness of VNC within specific clinical situations [20, 21, 25, 27, 28]. The rationale of replacing TNC by VNC images is to reduce radiation exposure by waiving the non-enhanced acquisition. It serves also when the non-contrast acquisition was erroneously omitted.

In the absence of previous demonstration in the literature, we conducted this study to assess whether VNC images could replace TNC images for aortic IMH diagnosis in AAS imaging protocols, by performing phantom and clinical experiments.

Material and methods

Study design

This work consisted of an in vitro phantom study performed in an academic hospital (Hôpital Louis Pradel, Lyon) and an in vivo clinical study carried out in two academic hospitals (Hôpital Louis Pradel, Lyon, and Clinique Universitaire UCL, Brussels) and approved by the Institutional Review Board of both institutions. The patients were included retrospectively; their data were anonymized and no informed consent was required.

Dual-layer dual-energy CT

This study was carried out on a single source dual-layer spectral CT (IQon, Philips Healthcare) equipped with two separate scintillator layers. The top layer absorbs the low-energy photons and the bottom layer the high-energy ones. Therefore, both acquisitions are perfectly simultaneous and the spectral separation is not compromised by any motion. An original feature of this technology is that it allows processing spectral data without having to select a dual-energy protocol prior to an examination and delivers the same dose as a conventional single-source CT [19, 22].

Phantom study

IMH phantom

To compare the TNC and VNC image quality, a custom IMH phantom was built using animal tissue and blood (Fig. 1). Experimental details are provided in the Supplemental data.

Image acquisition and reconstruction

The acquisition was carried out using a non-ECG gating aortic protocol (Table 1). The acquisitions were performed at three different CTDI*vol* (2.5, 5, and 10 mGy) without automatic current modulation in order to keep the dose constant between different phantoms. These exposure levels were chosen to match clinical AAS imaging protocols and correspond to a dose right index at 15, 21, 27 and 6, 12, 18 for the small and large phantoms, respectively. Each acquisition was repeated three times and the standard deviations and ranges of the averaged attenuation values were calculated. Conventional TNC images of the non-contrast phantoms, VNC images of the contrast phantoms, and "iodine no water" images were reconstructed using the proprietary iDose/Spectral iterative reconstruction algorithm at levels 0 and 3 and obtained directly from commercial software (Spectral Philips IntelliSpace Portal 9.0). To obtain the VNC images, the reconstruction algorithm subtracts the respective iodine component from each of the base components and creates a monoenergetic 70 keV from the resulting base components [19]. Level 0 corresponds closely to an FBP reconstruction with a minimum of additional iterative post-processing.

Image analysis

Images were analyzed on a clinical workstation with commercial software (Spectral Philips Intellispace Portal 9.0). Regions of interest (ROIs) of 0.8 to 2.0 cm^2 were drawn within the hematoma, blood, and fat by a radiologist with 6 years of experience in cardiovascular imaging (SSM) to measure the mean attenuation values and standard deviations (SD). After carefully matching each set of acquisition in the *z*-direction, the ROIs were copied/pasted on the corresponding slice. The absolute mean attenuation difference between TNC and VNC attenuation values was calculated. The contrast-to-noise ratio (CNR) between blood and hematoma on both images was calculated for each conditions using the formula below:

$$\mathrm{CNR} = \frac{|\text{Mean HU (hematoma)} - \text{Mean HU (blood)}|}{\text{SD (fat)}}$$

The SD of the fat attenuation surrounding the IMH model was chosen to assess image noise because of the homogeneity of this tissue. The water-equivalent diameters (WED) of the phantoms and the patients were calculated using custom software.

Clinical study

Patient characteristics

We retrospectively reviewed clinical and imaging data for patients who were suspected of having an acute aortic syndrome and who underwent a CTA between April 2017 and November 2018. The inclusion criterion was the presence of an isolated intramural hematoma confirmed by the surgery. When surgery had been declined, the diagnosis was based on a final consensus between the clinical signs and the imaging findings on CTA. Patients who underwent a single-phase CTA examination were excluded from the study. Taken together, 21 patients were included. The information about the population included in the study is shown in Table 2.

Image acquisition and reconstruction

All patients underwent a dual-phase CT according to the European Society of Cardiology 2014 guidelines on the diagnosis and treatment of aortic disease [9] (Table 1). For the arterial phase, bolus tracking and retrospective ECG gating were used following intravenous administration of 60–

Fig. 1 Representation of the aortic intramural hematoma (**a**) and anthropomorphic (**b**, **c**) phantoms. The false and inner lumen were filled with blood with extra iodinated contrast media for the inner lumen to target an attenuation value of 80 HU and 350 HU, respectively. Obese patients were simulated by adding an outer extension ring (**b**)

Table 1 Acquisition and reconstruction parameters for phantom and clinical studies

	Parameters	Phantom study	Clinical study
Acquisition	Tube potential (kVp)	120	120
	Detector collimation	64 × 0.625	64 × 0.625
	Pitch	1.234	1.234
	Rotation time (s)	0.27	0.27
	Exposure control	None	3D modulation
Reconstruction	Filter	B	B
	Section thickness (mm)	1.5	1.5
	Field of view (mm)	300	300

80 mL of iodinated contrast medium (3–3.5 mL/s) followed by 25 mL of physiologic saline solution. The image reconstructions for all patient included TNC, VNC, and "iodine no water" images, at iDose/Spectral level range 3.

Quantitative analysis

The images were analyzed similarly to what has been performed for the in vitro study. For each patient, a stack of 3 contiguous slices of 1.5 mm width was drawn at different positions separated by 15 mm depending on the IMH size. Measurements were performed within three different tissues: hematoma, blood, and peri-aortic or peri-abdominal fat. The CNRs were calculated as described above.

Qualitative analysis

Two radiologists (SSM, DR) with 6 years of experience in cardiovascular imaging as well as respectively 4 years (SSM) and no experience (DR) in dual-layer dual-energy CT (DL-DECT) images read the patients' cases. The readers were not blinded to the type of images and scored them for each patient at 4 different levels. The readers could change settings and window according to their personal preferences. The readers were asked to score the diagnostic confidence of the hyper-attenuation of the aortic wall relative to the blood pool based on a scale from 1 to 4: 1 = non-diagnostic, 2 = limited, 3 = diagnostic, and 4 = exemplary (Fig. 2) [29].

Radiation dose

The dose-length product (DLP) and volumic CT dose index (CTDI*vol*) for the non-contrast and contrast acquisitions were recorded. The effective dose (ED) was calculated as follows: ED = DLP × 0.014 (Thorax conversion factor) [30].

Statistical analysis

Statistical analyses were performed using the software R (R Foundation for Statistical Computing) [31]. All data are given as mean ± SD (1st quartile; 3rd quartile). Attenuation and CNR values were compared using a paired *t* test as the

Table 2 Patient characteristics (population, clinical data, radiation dose data). Data are represented with mean values ± standard deviation (1st quartile–3rd quartile)

	Criteria	Population
Population	Patients (*n*)	21
	Age (years)	70.2 ± 12.8 (63.7–78.3)
	Gender	8M, 13F
	BMI (m/kg^2)	24.8 ± 4.9 (21.3–29.1)
	WED (cm)	25.8 ± 5.0 (21.2–30.4)
Clinical data	IMH type (Stanford)	14A, 7B
	IMH thickness (mm)	7.0 ± 3.4 (5.0–8.6)
	Surgery	13
	Delay between CT and onset of AAS (days)	13.4 ± 38.2 (0.0–9.0)
Radiation dose data	$CTDI_{TNC}$ (mGy)	8.3 ± 6.1 (6.1–9.3)
	$CTDI_{VNC}$ (mGy)	11.3 ± 6.1 (7.1–13.5)
	mAs_{TNC}	110.1 ± 67.5 (67.0–113.0)
	mAs_{VNC}	135.1 ± 67.9 (83.0–180.0)
	Overall DLP (mGy cm)	1016.6 ± 753.7 (682.0–1130.1)
	Effective dose (mSv)	14.2 ± 10.6 (9.5–15.8)

hypothesis of normality of data distribution was met (D'Agostino-Pearson test, $p < 0.05$). The Wilcoxon signed-rank test for paired samples was applied to test for the quality difference between the TNC and VNC images. A p value < 0.05 was considered statistically significant. The inter-rater reliability between radiologists was calculated using a standard quadratic weighted Kappa test (poor, $k = 0.00–0.20$; fair, $k = 0.21–0.40$; moderate, $k = 0.41–0.60$; good, $k = 0.61–0.80$; or excellent, $k = 0.81–1.00$).

Results

Phantom study

The aortic wall hyper-attenuation was observed for all phantoms on both TNC and VNC images but not on the contrast-enhanced images (Fig. 3). On both TNC and VNC images, the hematoma and blood exhibited different attenuation values allowing to differentiate one from the other with either method (Table 3). We evaluated the effects of the ring, radiation dose, and iDose/Spectral level and found that while no significant difference in attenuation was observed for the TNC images in neither of them, a higher radiation dose or a smaller phantom was associated with higher attenuation values in both hematoma and blood in VNC images ($p < 0.001$) (Table 3 and Supplemental Figure 1). Additionally, the noise was higher in TNC images for all phantoms, radiation dose, and iDose conditions (Supplemental Table 1). Finally, we found similar hematoma, blood and fat attenuation values between the three repeated acquisitions, showing good inter-scan reproducibility (Supplemental Table 2).

Clinical study

Similar to the phantom study, the aortic IMH was not visible on contrast images, while it was clearly distinguishable on both TNC and VNC images. This result is illustrated in Fig. 4. Moreover, no significant differences in attenuation values were found between the TNC and VNC images for the blood or the hematoma among the 165 evaluated slices (Table 4). The noise was significantly lower in VNC images than in TNC images ($noise_{VNC} = 17.8 \pm 6.9$ [12.2; 22.5], $noise_{TNC} = 19.6 \pm 7.5$ [14.6; 23.8], $p < 0.0001$).

Contrast-to-noise ratio

Phantom study Figure 3 shows the results for the phantom conditions closest to clinical settings, that is to say small phantom (similar WED than clinical study), CTDI*vol* 10 mGy, and iDose 3, while the supplemental Figure 2 shows the results for all phantoms, iDoses, and CTDI*vol* conditions, individually. Altogether, for all conditions, the CNR values were not significantly different between the TNC and VNC images ($p > 0.05$) for both small and large phantoms (Supplemental Figure 2) except with the small phantoms under similar clinical conditions ($p > 0.0001$) (Fig. 5b).

Clinical study The CNR values were significantly higher in VNC images compared with those in TNC images as a result of lower noise in the VNC images and similar attenuation values between VNC and TNC images ($CNR_{VNC} = 1.07 \pm 0.82$ [0.68; 1.28], $CNR_{TNC} = 0.90 \pm 0.73$ [0.45; 1.29], $p = 0.018$, 95% confidence interval = [0.86; 1.28] and [0.71; 1.09], respectively) (Fig. 5).

Iodine concentration

The mean iodine concentrations (mg/mL) in patients were at 13.87 ± 5.73 (10.50; 17.05) within the blood. The mean apparent concentrations were at 0.55 ± 0.35 (0.22; 0.85) within the hematoma. The mean iodine concentrations (mg/mL) in vitro for 2.5, 5, and 10 mGy were respectively 0.94, 0.95, and 0.94 in the small phantom and 1.41, 1.75, and 1.57 in the large phantom within the hematoma and 10.07, 10.08, and 10.01 in the small phantom and 9.44, 9.36, and 9.26 in the large phantom within the blood. The mean iodine concentration in control tissue (fat) was 0.00 ± 0.01 (−0.01; 0.02) in both phantoms and 0.02 ± 0.10 (−0.04; 0.06) in the clinical study.

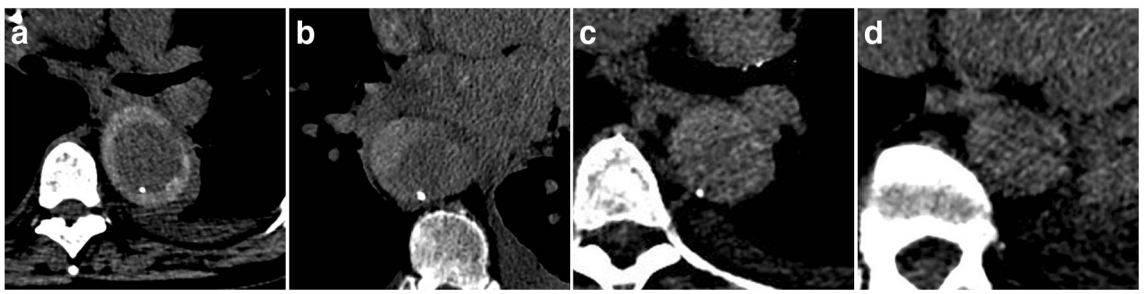

Fig. 2 Examples of diagnostic confidence rate (exemplary (**a**), diagnostic (**b**), limited (**c**), non-diagnostic (**d**)) (WL, 80; WW, 160)

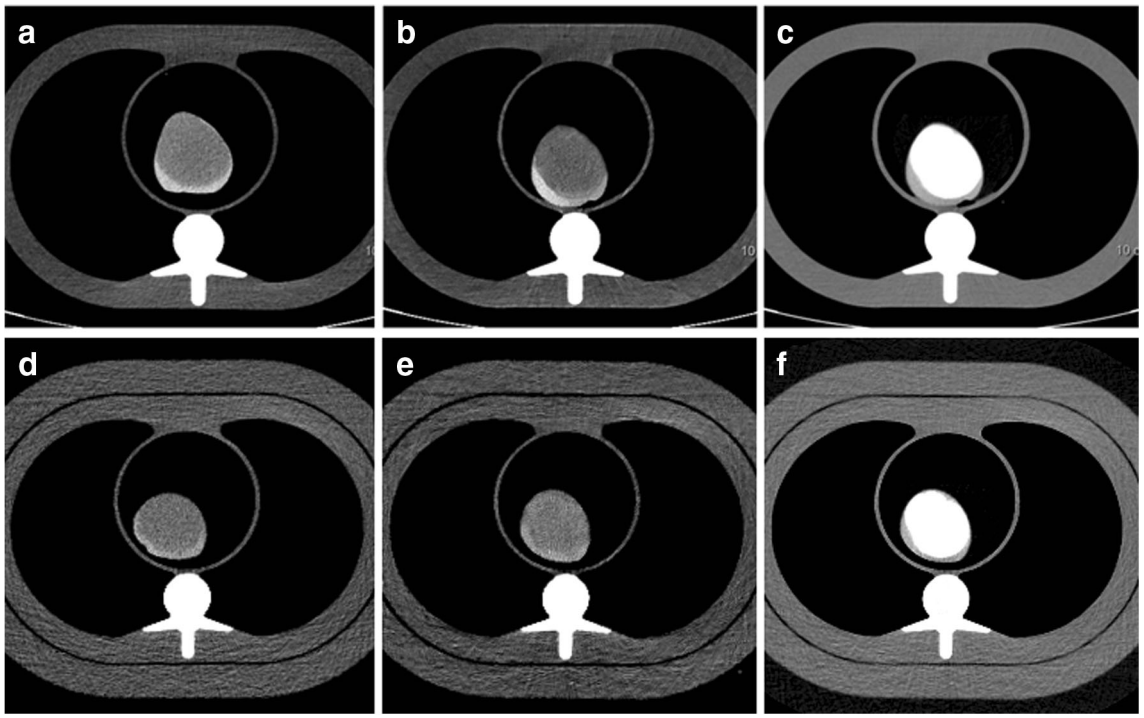

Fig. 3 CT scan of the in vitro IMH: the aortic wall hyper-attenuation in the phantom could be observed on the TNC (**a**, **d**) and VNC (**b**, **e**) images but not on the contrast images (**c**, **f**) for the small (**a**–**c**) as well as the large (**d**–**f**) phantoms (WL, 100; WW, 350)

Diagnostic confidence

The diagnostic confidence scores were close to exemplary for both the TNC and VNC images and were not significantly different between the two (TNC = 3.13 ± 0.74; VNC = 3.22 ± 0.73, $p > 0.30$). The inter-radiologists agreement was high for both images with TNC = 96.51%, $k = 0.87$; VNC = 93.80%, $k = 0.76$, as well as for the intra-radiologist reliability with TNC = 98.07%, $k = 0.87$; VNC = 96.74%, $k = 0.90$.

Radiation dose

The calculated effective doses (mSv) were 5.5 ± 3.7 (3.7; 6.3) and 8.8 ± 7.2 (4.3; 11.0), respectively, for non-contrast and contrast scans leading to an overall dose of 14.2 ± 10.6 (9.5–15.8) (Table 2). By suppressing TNC acquisition and using VNC, mean effective dose reduction would be 39.9 ± 10.8% (33.1; 44.0).

Discussion

In the present study, we demonstrated that using a DL-DECT system, it is possible to replace TNC images with VNC images and obtain reliable aortic IMH diagnosis while delivering lower doses of radiation than a typically dual-phase CT AAS protocol. The CNRs were comparable in both images between the hematoma and the blood allowing for the visualization of the relative hyper-attenuation of the hematoma in clinical study and also for every experimental condition of the in vitro study despite WED variations, CTDI*vol* differences, and iDose level choices.

In both studies, the attenuation values in the VNC images were slightly different than in the TNC images (up to ~ 10 HU). Such differences are expected since the VNC images mimic a monoenergetic image at 70 keV of non-contrast acquisition while TNC values are derived from conventional polychromatic images. HU values of conventional images are impacted by the beam-hardening effect: tube kVp, post-tube

Table 3 Hematoma and blood attenuation values for the small phantom in TNC and VNC images with conditions closest to clinical settings (similar WED than clinical study), CTDI*vol* 10 and iDose 3

Phantom	Images	$Attenuation_{hematoma}$ (HU)	$Attenuation_{blood}$ (HU)	*p*
Small	TNC	88.8 ± 0.8 (88.3–88.8)	56.4 ± 0.33 (79.3–79.5)	0.0001
	VNC	79.4 ± 0.3 (79.3–79.5)	47.6 ± 0.2 (47.6–47.7)	0.0002
Large	TNC	83.5 ± 0.66 (83.1–83.9)	55.8 ± 2.8 (53.8–57.6)	0.0002
	VNC	80.9 ± 1.2 (80.5–81.3)	52.1 ± 0.6 (51.8–52.5)	0.0001

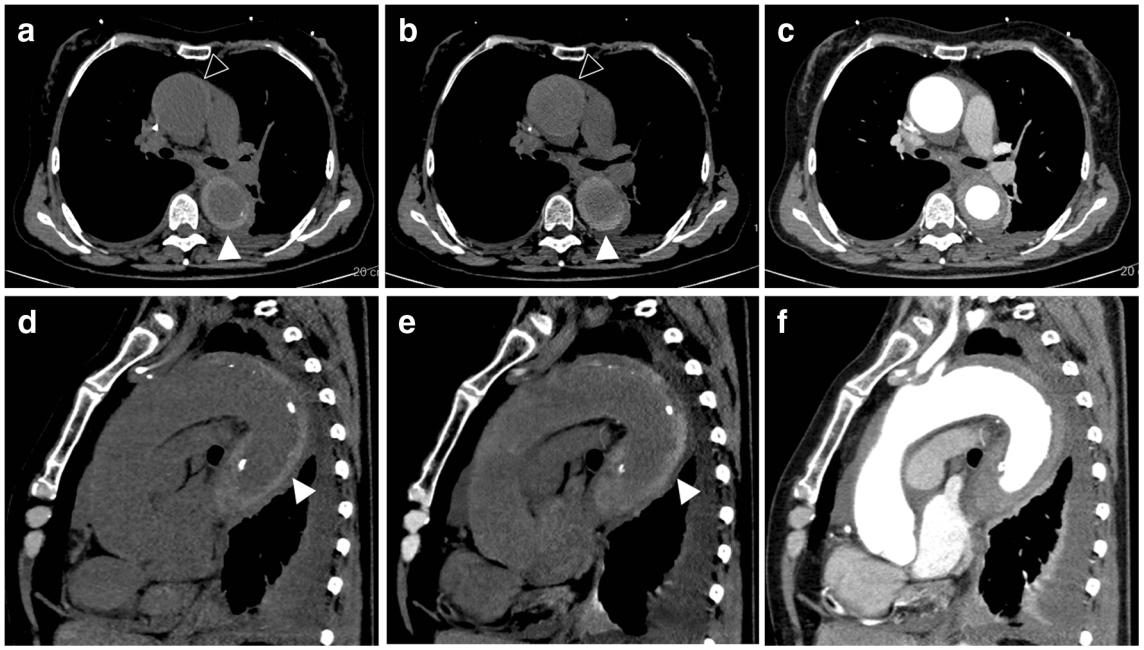

Fig. 4 CT scan of a 64-year-old patient diagnosed with aortic IMH (full arrowheads) on the TNC (**a**, **d**) and VNC (**b**, **e**) images, which was hardly visible at the level of the ascending aorta (empty arrowheads), especially on the contrast images (**c**, **f**), where its presence was later confirmed during the surgery (WL, 100; WW, 350)

filtration, and patient size. By definition, monoenergetic images are virtually free from such beam-hardening effects. Indeed, the VNC attenuation values in the two different phantom sizes are more consistent compared with the conventional TNC values.

In the phantom study, the attenuation values in the VNC images were lower than in the TNC images. This difference was accentuated at low-dose levels and phantom size, in agreement with previous studies [19, 22]. This could be explained by two factors. First, in DECT, the VNC images are derived from the water components based on a material decomposition between two components (water-iodine) in which any deviation from water-like attenuation is interpreted as non-zero iodine component [19, 22]. Therefore, their attenuation values end up being decreased. For example, as for bones, the calcifications are interpreted as a mixture of water-like and iodine-like materials, and the VNC algorithm does not separate the bone from iodine, explaining that the attenuation value of bone or calcification in VNC images is roughly half of their value in the original 70-keV image. Similarly, the elevated protein, iron, and hemoglobin content in the hematoma and blood, which increases the x-ray attenuation [32], is interpreted as a mixture of water-like and iodine-like material. Hence, the iodine content is overestimated which leads to an underestimation of the hematoma and blood attenuation in the VNC image. Second, in low-dose conditions (obese patients, low CTDI*vol*), the accuracy of iodine quantification is biased which, as demonstrated in several studies, also results in inaccurate attenuation values [22, 33]. However, in such cases, we found similar CNR probably explained by the noise suppression algorithms included in spectral reconstructions which take advantage of known statistical properties of the noise (anti-correlation between the two base images) to target it and reduce it [22, 34].

In the clinical study, we found slightly different results in comparison with the phantom study due to the difficulties mimicking perfectly the hematoma composition, as well as the heterogeneity of hematoma attenuation between patients. Firstly, the attenuation values were closer between VNC and TNC images in vivo, probably explained by the lower

Table 4 Attenuation and noise values in HU. Data are represented with mean values ± standard deviation (1st quartile–3rd quartile). Mean absolute differences were calculated between TNC and VNC images

Criteria	TNC	VNC	*p*
$Attenuation_{hematoma}$ (HU)	54.8 ± 7.4 (50.9–59.5)	55.2 ± 8.5 (49.1–60.2)	0.440
$Attenuation_{blood}$ (HU)	40.3 ± 5.9 (36.5–43.6)	39.2 ± 7.0 (35.9–43.7)	0.071
Mean absolute $difference_{hematoma}$ (HU)	5.0 ± 4.2		NA
Mean absolute $difference_{blood}$ (HU)	4.7 ± 3.9		NA
Noise (HU)	19.6 ± 6.0 (16.2–23.5)	18.1 ± 6.3 (13.2–22.2)	0.041

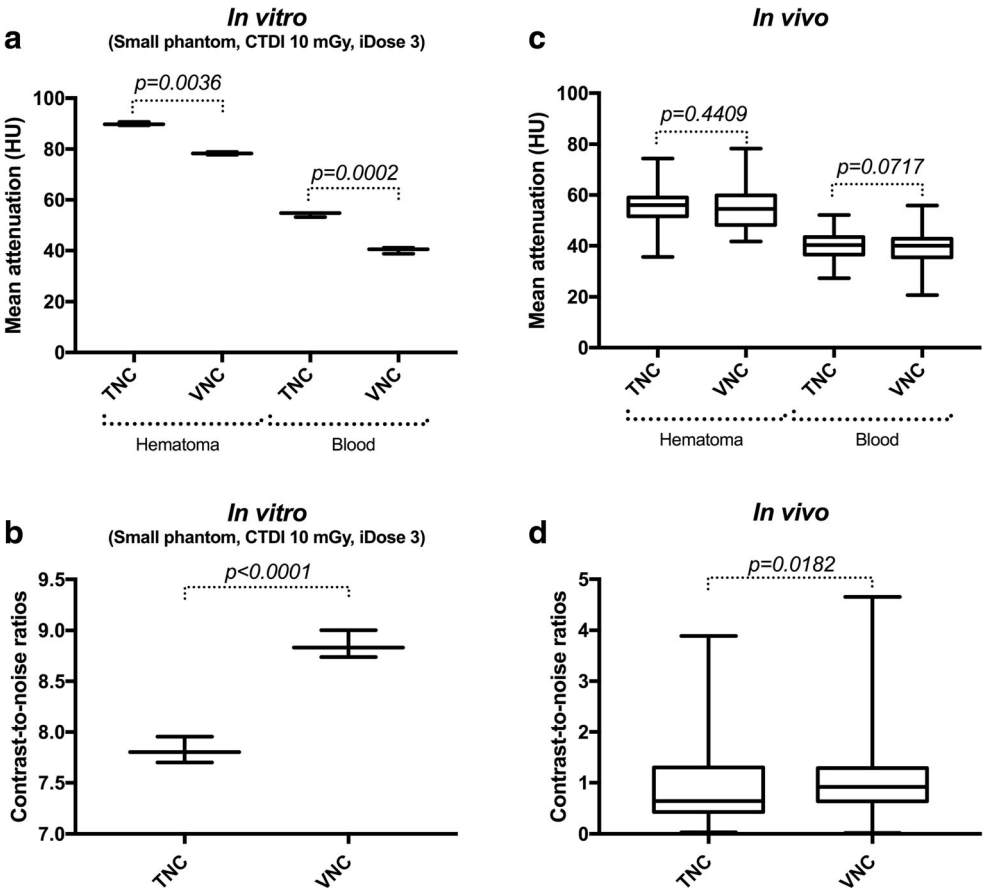

Fig. 5 Distribution of the in vitro (**a**, **b**) and in vivo (**c**, **d**) mean CT attenuation values and contrast-to-noise ratios shown as boxplots. The lower and upper margins of each box indicate the 25th and 75th percentile. Median is marked by the line in the box, and outliers indicate the minimal and maximal values

concentrations of hemoglobin, protein, and iron. Indeed, the mean attenuations for hematoma and blood were lower in vivo than in vitro. This decreased the overestimation of the iodine content, as confirmed by the lower iodine concentrations present in the hematoma, which led to a greater estimation of hematoma attenuations in the VNC images. Secondly, the percentages of absolute differences measurements of less than 5, 10, and 15 HU were found in more than 70, 92, and 98% of the cases, respectively, in line with recent studies [24, 35]. Finally, there was a significant difference in CNR between VNC and TNC images. This result was most likely due to the different doses of radiation that were used between the non-contrast and contrast acquisitions.

An important result of our work is the similar diagnostic confidence for the hyper-attenuation of the aortic wall relative to the blood pool on VNC compared with TNC images, independently from the experience of the readers to DL-DECT images. This finding, combined with the enhanced CTA, would then end up with a similar diagnostic performance of IMH to a standard CT protocol with two acquisitions. We also observed good and excellent inter-rater agreement for the VNC and TNC images, respectively. This contrasts with previous studies that demonstrated inhomogeneous subtraction of iodine in VNC images [20, 36, 37]. We can explain our results by a better correction of the beam hardening and management of the high iodine concentrations. Indeed, we took advantage of a recent software update of the DL-DECT system that improves image quality.

Altogether, our data appear to be consistent with previous studies from other fields that reported comparable quality between VNC and TNC images [20, 21, 23, 28]. However, it is the first study to evaluate VNC images obtained from clinically acquired examinations in an acute condition setting. In addition, AAS have variable clinical presentations that may overlap with other acute cardiovascular events (e.g., myocardial infarction, pericarditis) that are more frequent and only require enhanced CT to be diagnosed. Unfortunately, IMH can be diagnosed only if an unenhanced CT has been done first. Therefore, when a radiologist is unexpectedly confronted to a thickened aortic wall on an enhanced CT, it is not possible to reliably diagnose IMH. On the contrary, using DL-DECT, it would be possible to use VNC images a posteriori and look for hyper- attenuation relative to the blood pool to diagnose IMH. This protocol also has the advantage of substantially decreasing the radiation dose as shown here as well as in other studies [20, 36].

Our work has some limitations such as static blood in the phantom aortic lumen led to a greater heterogeneity of the attenuation values. Secondly, our phantom, by the high

attenuation found in the hematoma, was not reflecting the full range attenuations of IMH. However, the acute ones were well reflected. Finally, while the patients included in the study represented a heterogeneous panel of the population with a great diversity of WEDs and $CTDI_{vol}$, there were still only 21 subjects.

In conclusion, we demonstrate in the present study that it is possible to use VNC images from DECT to diagnose IMH while potentially decreasing the dose of radiation delivered to the patients.

Acknowledgments We thank Pr. Emmanuel Coche, Dr. Begum Demirler, and Dr.Matteo Pozzi for helping with the clinical study.

Funding This work has not received any funding.

Compliance with ethical standards

Guarantor The scientific guarantor of this publication is Professor Loic Boussel.

Conflict of interest Philippe Coulon, Yoad Yagil, and Nadav Shapira are employees of Philips Healthcare, the manufacturer of the scanner.

Statistics and biometry Prof. Loic Boussel provided statistical advice for this manuscript.

Informed consent Written informed consent was waived by the Institutional Review Board.

Ethical approval Institutional Review Board approval was not required.

Methodology
- Retrospective
- Observational
- Multicenter study

References

1. Mussa FF, Horton JD, Moridzadeh R, Nicholson J, Trimarchi S, Eagle KA (2016) Acute aortic dissection and intramural hematoma: a systematic review. JAMA 316:754–763
2. Hiratzka LF, Bakris GL, Beckman JA et al (2010) 2010 ACCF/AHA/AATS/ACR/ASA/SCA/SCAI/SIR/STS/SVM guidelines for the diagnosis and management of patients with Thoracic Aortic Disease: a report of the American College of Cardiology Foundation/American Heart Association Task Force on Practice Guidelines, American Association for Thoracic Surgery, American College of Radiology, American Stroke Association, Society of Cardiovascular Anesthesiologists, Society for Cardiovascular Angiography and Interventions, Society of Interventional Radiology, Society of Thoracic Surgeons, and Society for Vascular Medicine. Circulation 121:e266–e369
3. Bhalla S, West OC (2005) CT of nontraumatic thoracic aortic emergencies. Semin Ultrasound CT MR 26:281–304
4. Romano L, Pinto A, Gagliardi N (2007) Multidetector-row CT evaluation of nontraumatic acute thoracic aortic syndromes. Radiol Med 112:1–20
5. Song JK (2011) Aortic intramural hematoma: aspects of pathogenesis 2011. Herz 36:488–497
6. Vilacosta I, San Román JA, Ferreirós J et al (1997) Natural history and serial morphology of aortic intramural hematoma: a novel variant of aortic dissection. Am Heart J 134:495–507
7. Manghat NE, Morgan-Hughes GJ, Roobottom CA (2005) Multidetector row computed tomography: imaging in acute aortic syndrome. Clin Radiol 60:1256–1267
8. Vardhanabhuti V, Nicol E, Morgan-Hughes G et al (2016) Recommendations for accurate CT diagnosis of suspected acute aortic syndrome (AAS)–on behalf of the British Society of Cardiovascular Imaging (BSCI)/British Society of Cardiovascular CT (BSCCT). Br J Radiol 89:20150705
9. Erbel R, Aboyans V, Boileau C et al (2014) ESC guidelines on the diagnosis and treatment of aortic diseases: document covering acute and chronic aortic diseases of the thoracic and abdominal aorta of the adult. The task force for the diagnosis and treatment of aortic diseases of the European Society of Cardiology (ESC). Eur Heart J 35:2873–2926
10. Sodickson A, Baeyens PF, Andriole KP et al (2009) Recurrent CT, cumulative radiation exposure, and associated radiation-induced cancer risks from CT of adults. Radiology 251:175–184
11. Brenner DJ, Hall EJ (2007) Computed tomography–an increasing source of radiation exposure. N Engl J Med 357:2277–2284
12. Knollmann FD, Lacomis JM, Ocak I, Gleason T (2013) The role of aortic wall CT attenuation measurements for the diagnosis of acute aortic syndromes. Eur J Radiol 82:2392–2398
13. Godwin JD, Breiman RS, Speckman JM (1982) Problems and pitfalls in the evaluation of thoracic aortic dissection by computed tomography. J Comput Assist Tomogr 6:750–756
14. McCollough CH, Leng S, Yu L, Fletcher JG (2015) Dual- and multi-energy CT: principles, technical approaches, and clinical applications. Radiology 276:637–653
15. Altman A, Carmi R (2009) A double-layer detector, dual-energy CT — principles, advantages and applications. Med Phys 36:2750
16. Fleischmann D, Boas FE (2011) Computed tomography–old ideas and new technology. Eur Radiol 21:510–517
17. Sellerer T, Noël PB, Patino M et al (2018) Dual-energy CT: a phantom comparison of different platforms for abdominal imaging. Eur Radiol 28:2745–2755
18. Qin L, Gu S, Chen C et al (2019) Initial exploration of coronary stent image subtraction using dual-layer spectral CT. Eur Radiol. https://doi.org/10.1007/s00330-018-5990-1
19. Hua CH, Shapira N, Merchant TE, Klahr P, Yagil Y (2018) Accuracy of electron density, effective atomic number, and iodine concentration determination with a dual-layer dual-energy computed tomography system. Med Phys 45:2486–2497
20. Sauter AP, Muenzel D, Dangelmaier J et al (2018) Dual-layer spectral computed tomography: virtual non-contrast in comparison to true non-contrast images. Eur J Radiol 104:108–114
21. Graser A, Johnson TR, Hecht EM et al (2009) Dual-energy CT in patients suspected of having renal masses: can virtual nonenhanced images replace true nonenhanced images? Radiology 252:433–440
22. Ehn S, Sellerer T, Muenzel D et al (2018) Assessment of quantification accuracy and image quality of a full-body dual-layer spectral CT system. J Appl Clin Med Phys 19:204–217
23. Lehti L, Söderberg M, Höglund P, Nyman U, Gottsäter A, Wassélius J (2018) Reliability of virtual non-contrast computed tomography angiography: comparing it with the real deal. Acta Radiol Open 7:2058460118790115
24. Toepker M, Moritz T, Krauss B et al (2012) Virtual non-contrast in second-generation, dual-energy computed tomography: reliability of attenuation values. Eur J Radiol 81:e398–e405
25. Cha D, Kim CK, Park JJ, Park BK (2016) Evaluation of hyperdense renal lesions incidentally detected on single-phase post-contrast CT using dual-energy CT. Br J Radiol 89:1062

26. Yoo SY, Kim Y, Cho HH et al (2013) Dual-energy CT in the assessment of mediastinal lymph nodes: comparative study of virtual non-contrast and true non-contrast images. Korean J Radiol 14: 532–539
27. Aran S, Daftari Besheli L, Karcaaltincaba M, Gupta R, Flores EJ, Abujudeh HH (2014) Applications of dual-energy CT in emergency radiology. AJR Am J Roentgenol 202:W314–W324
28. Tijssen MPM, Hofman PA, Stadler AAR et al (2014) The role of dual energy CT in differentiating between brain haemorrhage and contrast medium after mechanical revascularisation in acute ischaemic stroke. Eur Radiol 24:834–840
29. European guidelines on quality criteria for computed tomography. Available via http://drs.dk/guidelines/ct/quality/mainindex.htm. Last accessed 24 May 2019
30. Si-Mohamed S, Greffier J, Bobbia X et al (2017) Diagnostic performance of a low dose triple rule-out CT angiography using SAFIRE in emergency department. Diagn Interv Imaging 98:881–891
31. R Core Team (2018). R: A language and environment for statistical computing. R Foundation for Statistical Computing, Vienna, Austria
32. New PF, Aronow S (1976) Attenuation measurements of whole blood and blood fractions in computed tomography. Radiology 121:635–640
33. Kim H, Goo JM, Kang CK, Chae KJ, Park CM (2018) Comparison of iodine density measurement among dual-energy computed tomography scanners from 3 vendors. Invest Radiol 53:321–327
34. Park KK, Oh CH, Akay M (2011) Image enhancement by spectral-error correction for dual-energy computed tomography. Conf Proc IEEE Eng Med Biol Soc 2011:8491–8494
35. Ananthakrishnan L, Rajiah P, Ahn R et al (2017) Spectral detector CT-derived virtual non-contrast images: comparison of attenuation values with unenhanced CT. Abdom Radiol (N Y) 42:702–709
36. Sahni VA, Shinagare AB, Silverman SG (2013) Virtual unenhanced CT images acquired from dual-energy CT urography: accuracy of attenuation values and variation with contrast material phase. Clin Radiol 68:264–271
37. De Cecco CN, Buffa V, Fedeli S et al (2010) Dual energy CT (DECT) of the liver: conventional versus virtual unenhanced images. Eur Radiol 20:2870–2875